Auto-oscillating Spin-Wave Modes of Constriction-Based Spin Hall Nano-oscillators in Weak In-Plane Fields

Hamid Mazraati,[1,2,*] Seyyed Ruhollah Etesami,[3] Seyed Amir Hossein Banuazizi,[2] Sunjae Chung,[2,3] Afshin Houshang,[1,3] Ahmad A. Awad,[1,3] Mykola Dvornik,[1,3] and Johan Åkerman[1,2,3]

[1] *NanOsc AB, SE-164 40 Kista, Sweden*
[2] *Department of Applied Physics, School of Engineering Sciences, KTH Royal Institute of Technology, Electrum 229, SE-16440 Kista, Sweden*
[3] *Department of Physics, University of Gothenburg, SE-412 96 Gothenburg, Sweden*

(Received 9 June 2018; revised manuscript received 12 September 2018; published 7 November 2018)

We experimentally study the auto-oscillating spin-wave modes in $Ni_{80}Fe_{20}/\beta$-W constriction-based spin Hall nano-oscillators as a function of bias current, strength of the in-plane applied field, and azimuthal field angle in the low-field range of 40–80 mT. We observe two different spin-wave modes: (i) a linear-like mode confined to the internal field minima near the edges of the nanoconstriction, and only weakly dependent on the bias current and the applied-field angle, and (ii) a second, lower-frequency mode with significantly higher threshold current and stronger dependence on both the bias current and the external-field angle. Micromagnetic modeling qualitatively reproduces the experimental data and reveals that the second mode is a spin-wave bullet and that the spin Hall nano-oscillator mode hops between the two modes, resulting in a substantial increase in linewidths. In contrast to the linearlike mode, the bullet is localized in the middle of the constriction and shrinks with increasing bias current. Using intrinsic frequency doubling at zero field angle, we can reach frequencies above 9 GHz in fields as low as 40 mT, which is important for the development of low-field spintronic oscillators with applications in microwave-signal generation and neuromorphic computing.

DOI: 10.1103/PhysRevApplied.10.054017

I. INTRODUCTION

Spin-torque nano-oscillators—microwave-signal-generating devices based on spin-wave auto-oscillations—are of great interest for many kinds of nanoscale applications as they provide highly coherent and widely tunable microwave signals at room temperature [1]. Recently, they have been succeeded by so-called spin Hall nano-oscillators (SHNOs), which utilize the spin Hall effect [2–7] to generate microwave signals of similar quality [8]. A variety of SHNO geometries and material compositions have been proposed [8–20]. Most recently, a constriction-based SHNO was developed with the particular advantages of having a rather simple fabrication process and relatively low driving current [21]. Later, the mutual synchronization of multiple constriction-based SHNOs was experimentally demonstrated for strong oblique magnetic fields, and substantial improvements in the output power and quality factor were observed [22]. Thanks to the unprecedented ability of constriction-based SHNOs to phase-lock with each other, they may also be used for future spintronic neuromorphic computing devices [23,24]. However, most practical applications require these devices to operate in either zero or weak applied magnetic fields. A deeper understanding of the SHNO dynamics in such regimes is thus necessary for further developments.

Demidov *et al.* [21] demonstrated that for an in-plane field of 40 mT applied at 40° with respect to the drive current, constriction-based SHNOs exhibit a single auto-oscillating mode over a wide range of applied currents with weak negative-frequency tunability. Dvornik *et al.* [25] later showed that such auto-oscillations emerge from the linear localized mode (i.e., its frequency does not depend on its amplitude) [26] of the nanoconstriction. Although a transition to multimode operation with substantial line broadening was also reported in Ref. [21], it was not discussed in detail and the origin of the additional peaks was not explained. Finally, optimization of the in-plane field angle is essential to achieve high output power and robust mutual synchronization of these devices in in-plane fields [27].

In this work, we report angular-resolved measurements of constriction-based-SHNO microwave-signal generation in weak in-plane fields, H_{IP}. We observe both a linear-like mode confined to the minima of the internal field near

*mazraati@kth.se

 © 2018 American Physical Society

the edges of the nanoconstriction and a lower-frequency spin-wave bullet mode localized in the middle of the constriction. Our micromagnetic simulations suggest that the SHNO hops rapidly between these two modes, consistent with the much-larger linewidths observed in this regime. Finally, we use intrinsic frequency doubling to achieve frequencies exceeding 9 GHz in fields as low as 40 mT.

II. EXPERIMENT

A. Device fabrication and measurement setup

The SHNO stack, consisting of a $Ni_{80}Fe_{20}$(5 nm)/β-W(5 nm) bilayer, is prepared on a c-plane sapphire substrate by dc/rf magnetron sputtering in a 2.5-mTorr argon atmosphere in an ultrahigh-vacuum chamber (base pressure below 1×10^{-8} mTorr). It is then patterned into an array of 4×12 μm^2 rectangular mesas by photolithography and argon-ion milling. Nanoconstrictions with a width of 150 nm are subsequently fabricated in the center of these mesas by a combination of electron-beam lithography and dry etching. To determine the magnetic characteristics of the stack by spin-torque-induced-ferromagnetic-resonance (ST-FMR) measurements, 6-μm-wide bars are simultaneously fabricated next to the SHNOs. Finally, a conventional ground-signal-ground waveguide and electrical contact pads for broad-frequency-range microwave measurement are fabricated by lift-off photolithography and Cu/Au sputtering on top of both the nanoconstrictions and the bars.

Figure 1(a) shows a schematic of the device structure, including the directions of the applied in-plane field and current: the field angles $\varphi = 0^\circ$ and $+90^\circ$ are along the $+y$ axis and $+x$ axis, respectively. A negative (positive) current represents electrons flowing along the $+x$ $(-x)$ direction.

The magnetoresistance of the SHNO versus the in-plane field angle is shown in Fig. 1(b), revealing an anisotropic magnetoresistance (AMR) ratio of 0.26%, similar to literature values for thin NiFi films [28]. We perform ST-FMR measurements on bars using the homodyne-detection approach [12,29–33]. A 313-Hz pulse-modulated microwave signal is applied alongside a direct current through a bias tee, and the modulated signal is then detected through the same bias tee and analyzed with a lock-in amplifier. The applied field is swept from 250 to 0 mT, while the frequency of the input microwave signal and the level of the direct current are fixed.

Microwave measurements are performed in a custom-built setup. While a direct current is injected through the constriction area of the SHNO in an in-plane field, the auto-oscillation microwave signal is acquired by a spectrum analyzer after being amplified by 35 dB with a broadband low-noise amplifier. All measurements are performed at room temperature.

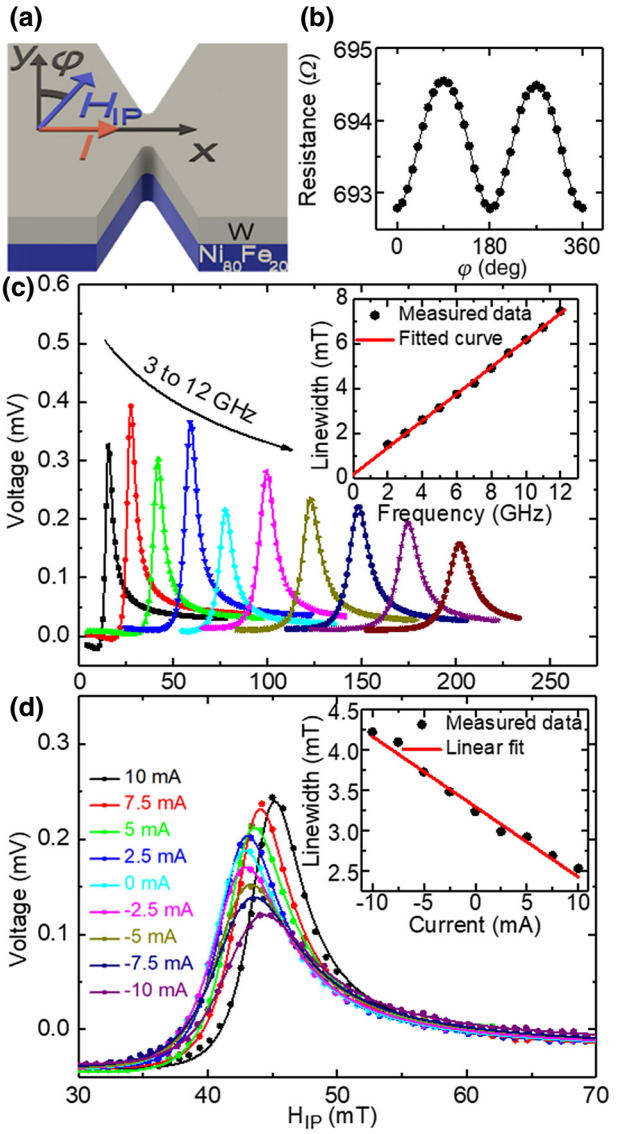

FIG. 1. (a) The nanoconstriction-based SHNO and the configuration of the in-plane field and the current, (b) the angle-dependent magnetoresistance of the stack, (c) ST-FMR peaks at $I_{dc} = 0$ mA for different microwave frequencies, and (d) ST-FMR peaks for $f = 5$ GHz at different direct currents. Solid lines show Lorentzian fits. The insets show the extracted linewidths of ST-FMR peaks and their linear fits.

B. Results

Figure 1(c) shows the ST-FMR spectra at different microwave frequencies from 3 to 12 GHz (dots), with each spectrum well fitted to a sum of one symmetric and one asymmetric Lorentzian (solid lines) [34]. The extracted frequencies of the resonance peaks fit well to the Kittel formula [35], leading to an effective magnetization of $\mu_0 M_{eff} = 0.71$ T and a gyromagnetic ratio of $\gamma/2\pi = 28$ GHz/T. The inset in Fig. 1(c) shows the extracted linewidths of the corresponding peaks (black dots) and

their fit to the linear model (solid red line). The value of the Gilbert damping obtained is $\alpha = 0.016$.

Figure 1(d) shows the ST-FMR spectra for a range of bias currents from +10 to −10 mA measured at a fixed microwave frequency of 5 GHz. The extracted-linewidth-versus-current behavior and a fit to the linear model [34,36,37] are shown in the inset. The extracted value of the spin Hall efficiency, defined as the ratio of the absorbed spin and charge current densities, is $\xi_{SH} = -0.385$, which is significantly higher than in the case of $Ni_{80}Fe_{20}$/Pt stacks [8–13,21,38].

The power spectral densities (PSDs) of the SHNO versus bias current for fields of 40, 60, and 80 mT applied $\varphi = 30°$ in plane are shown in Figs. 2(a)–2(c). For $\mu_0 H_{IP} = 80$ mT, there is a single dominant spin-wave mode that, according to Ref. [25], should originate from the linear magnonic edge mode of the constriction (hence the label "linearlike mode"). In contrast to the uniform ferromagnetic resonance of in-plane magnetized films, where the frequency decreases with the amplitude of precession, the observed auto-oscillations experience a nonmonotonic frequency-versus-current behavior. At lower currents, the frequency of the mode is almost constant, while its linewidth decreases with increasing current. However, at a certain field-dependent current, the mode shows a redshift (negative nonlinearity), and the linewidth starts to increase. At the same time, traces of a lower-frequency and larger-linewidth signal can be seen in Fig. 2(a). These are the signatures of the so-called spin-wave bullet—a nonlinear and nontopological self-localized mode nucleated in regions of negative nonlinearity [8,39–43]. They become more apparent when the applied field is reduced to 60 mT [Fig. 2(b)] and eventually dominate at 40 mT [Fig. 2(c)]. Our experimental data suggest that the contribution of the negative nonlinearity could increase with the applied field, shifting its onset current downward from approximately 1.4 mA at 40 mT to 1 mA at 80 mT.

Generally, the linearlike and the bullet modes cannot coexist when they overlap in space, so the presence of both signals in the measured spectra is likely due to mode hopping [41,44–48]. The reduced stability and broader linewidth of the bullet mode at higher fields indicate an increase in the nonlinearity and the suppression of the nonlinear magnetic losses [49] that limit the auto-oscillation amplitude [Fig. 2(d)].

The fundamental and second harmonics of both modes as a function of the in-plane angle of the applied field of constant strength, $\mu_0 H_{IP} = 40$ mT, are plotted in Figs. 3(a) and 3(b) at $I_{dc} = 1.3$ mA and 1.1 mA, respectively. The slight asymmetry of the responses with respect to the field angle is likely due to fabrication-related shape imperfections or the slight misalignment of the sample with respect to the center of the magnet. We observe no auto-oscillations for angles beyond $|\varphi| = 45°$, either because the edge modes (a) disappear due to the suppression of the spin-wave wells or (b) do not get excited as they move away from the constriction, experiencing less spin-current density. The former is unlikely since it would be accompanied by a considerable increase in frequency, which we do not see experimentally. The frequency of the linearlike mode depends only weakly on the in-plane angle of the applied field, suggesting minimal changes to its localization depth.

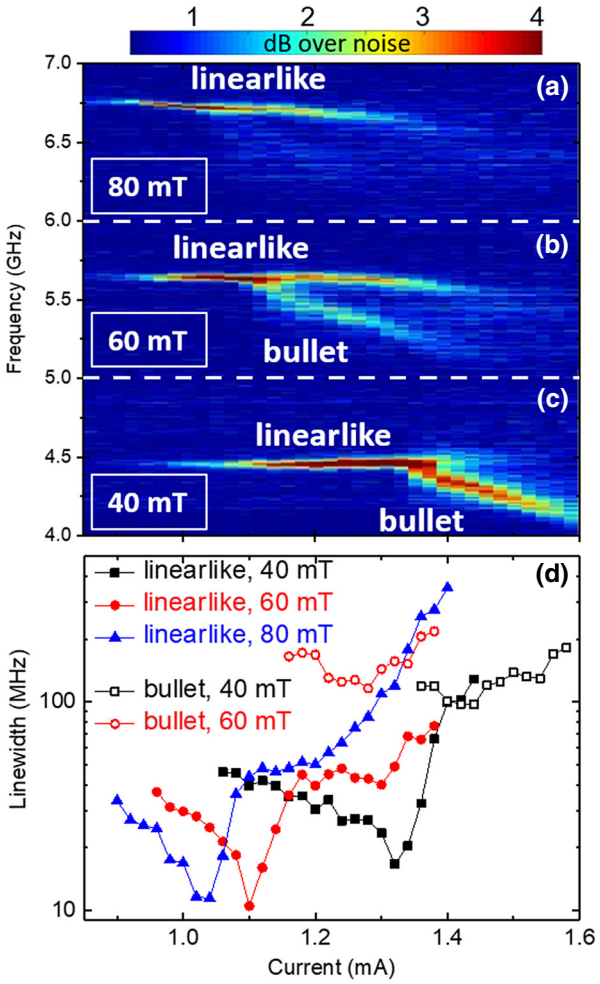

FIG. 2. Current-dependent auto-oscillation power spectral density for a field of (a) $\mu_0 H_{IP} = 0.04$ T, (b) $\mu_0 H_{IP} = 0.06$ T, and (c) $\mu_0 H_{IP} = 0.08$ T applied along $\varphi = 30°$. (d) Fitted linewidth of the corresponding resonant peaks.

The bullet mode is observed at higher currents [Fig. 3(a)], and disappears as the current drops [Fig. 3(b)], similar to the PSD maps shown in Fig. 2. In contrast to the linearlike mode, the frequency of the bullet mode depends strongly on the field angle and decreases with the angle of the external field. This may be attributed to the angular dependence of the dampinglike torque. At low angles, the magnetization vector points mostly antiparallel to the polarization of the spin current, resulting in higher

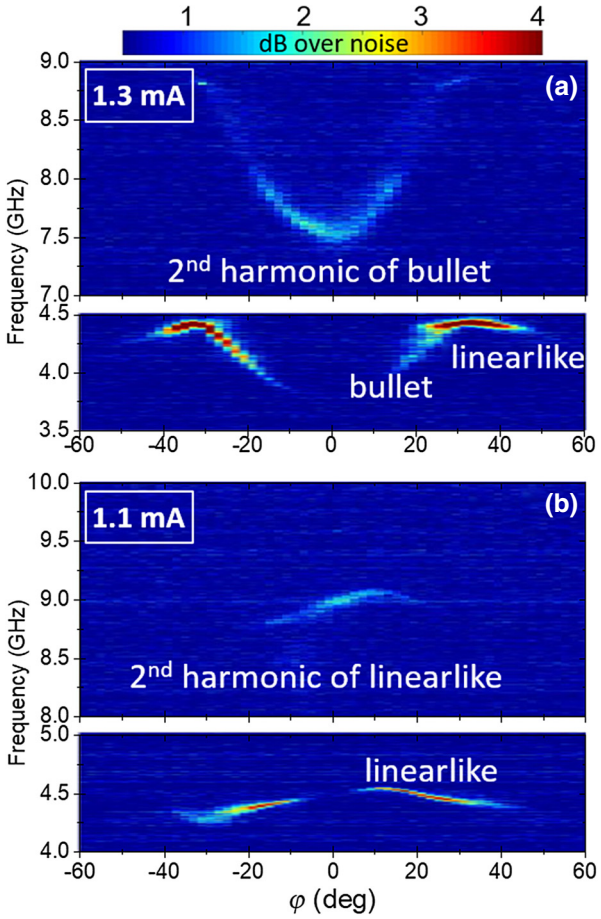

FIG. 3. PSD map of the fundamental and second harmonic of the modes versus the in-plane angle of the field for $\mu_0 H_{IP} = 40$ mT at (a) $I_{dc} = 1.3$ mA and (b) $I_{dc} = 1.1$ mA.

spin-torque efficiency, a larger bullet amplitude, and thus a greater nonlinear frequency redshift.

It is worth noting that the fundamental harmonic for any of the modes is not detected for small field angles. This is a consequence of the first derivative of the AMR curve [Fig. 1(b)] approaching zero at $\varphi = 0°$. However, both modes are instead clearly observed by their signals at twice their original frequencies, since the second derivative of the AMR curve has a maximum in the vicinity of $\varphi = 0°$ [50]. As a consequence, using this intrinsic frequency doubling, we can reach very high frequencies even at very low fields.

III. MICROMAGNETIC SIMULATIONS

To investigate the physics behind the experimentally observed spin-wave modes, we conduct micromagnetic simulations using MUMAX^3 [51]. The material parameters used in the simulations—such as the permalloy saturation magnetization, the Gilbert damping, the gyromagnetic ratio, and the spin Hall efficiency of the bilayer—are obtained directly from the ST-FMR measurements. An exchange stiffness of $A_{ex} = 10$ pJ/m is considered for permalloy [52]. We run the simulations for a geometry with a lateral size of 2000×2000 nm^2 (large enough to avoid boundary effects) and a thickness of 5 nm, which is similar to the thickness of the ferromagnetic layer in the real sample. The distributions of the direct charge current and the corresponding Oersted field are obtained with COMSOL MULTIPHYSICS [25] for a $Ni_{80}Fe_{20}$/W bilayer with resistivity of 0.90 $\mu\Omega$/m for permalloy and 2.12 $\mu\Omega$/m for W. The auto-oscillation spectra are obtained by application of a fast Fourier transform (FFT) to the net x component of the total magnetization, simulated over 1000 ns. We assume that the spin-current polarization equals $P = 1$ and is independent of the angle between the directions of magnetization and spin-current polarization.

The auto-oscillation spectra versus current, and the splitting into two modes can be seen in Fig. 4(a), in good agreement with our experimental observations [Fig. 2(b)]. We additionally calculate the linear eigenmodes of the SHNOs

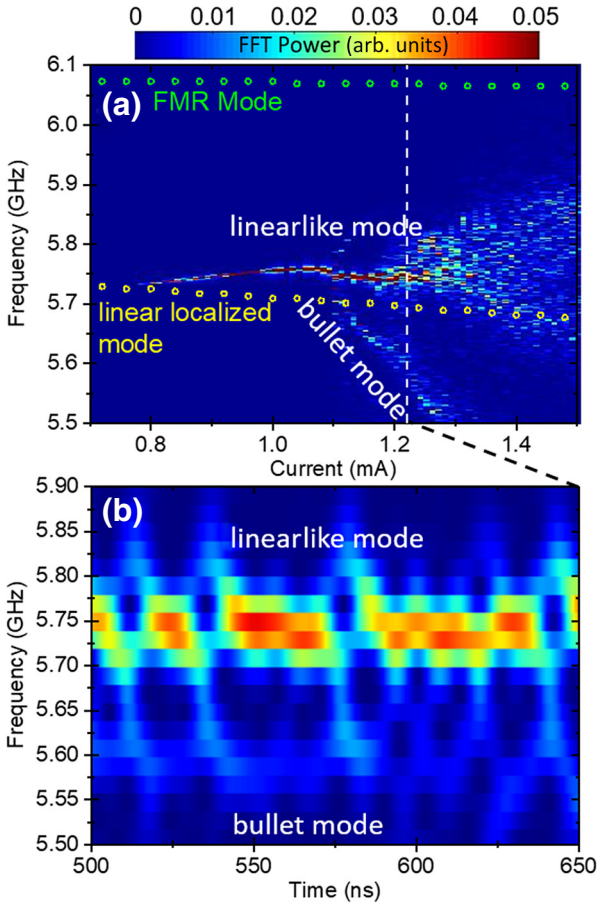

FIG. 4. Simulation. (a) FFT power color map of the total magnetization as a function of frequency and current at $\mu_0 H_{IP} = 60$ mT and $\varphi = 30°$. The eigenmodes, including the FMR and linear localized modes, are shown by green and yellow circles, respectively. (b) Spectrogram of total magnetization at $I_{dc} = 1.22$ mA.

by turning off the spin torque, while keeping the Oersted field, in our simulation and exciting the system with a magnetic field pulse (a sinc function with an amplitude of 0.5 mT and a duration of 25 ps). The FMR mode and the linear localized mode are shown in Fig. 4(a) by green and yellow circles, respectively. Both auto-oscillation modes are far below the FMR frequency (i.e., both are localized). In agreement with Ref. [25], the frequency of the auto-oscillation at its onset coincides with the eigenmode of the constriction. In clear contrast, the lower-frequency mode that emerges at around 1.1 mA cannot be attributed to the eigenmodes of the constriction, and hence not to any deepening of the spin-wave well caused by the Oersted field [21]. Instead, we conclude that the lower-frequency mode is a self-localized spin-wave bullet. In contrast to the in-plane-magnetized extended films—where bullets typically have lower threshold currents than the quasilinear propagating spin waves—they require higher currents than the linearlike modes of the constriction. This could be attributed to the fact that self-localization in the given volume occurs only when some critical number of magnons is achieved [39], while field confinement happens even for spin waves with vanishing amplitudes.

It is worth mentioning that the bullet appears to be splitting from the linearlike mode. We, therefore, inspect the transient behavior of the magnetization dynamics in a multimode regime ($I_{dc} = 1.22$ mA) by performing time-frequency analysis using a short-time Fourier transform. Because of the small frequency gap between the linearlike mode and the bullet mode, we do not decrease the moving window length to less than 50 ns so as to maintain a reasonable frequency resolution of 0.02 GHz (Kaiser window with $\beta = 30$ and overlap of 49.95 ns). As can be seen in Fig. 4(b), the discontinuities in the linearlike mode are followed by a sharp transition to the bullet mode (i.e., mode hopping is observed). We, therefore, conclude that the bullet mode does not branch off, but instead nucleates from the linearlike mode toward a lower frequency. To this end, it could be viewed as a self-localization of the field-localized mode of the constriction.

To determine the spatial distribution of the observed modes, we perform pointwise temporal FFT over the dynamic component of the magnetization sampled in the vicinity of the constriction; that is, mode-profile analysis using the SEMARGL-NG package [53,54]. The profiles of the linearlike and bullet modes calculated for an applied current of $I_{dc} = 1.26$ mA are shown in Figs. 5(a) and 5(b), respectively. While the linearlike mode is confined to the edges of the constriction where the internal field has local minima, the bullet mode is more localized in the center of the constriction, where the internal field instead has a local maximum. This again confirms its predominant self-localization character. Similarly to what was observed in Refs. [21,27], both the linearlike mode and the bullet mode mostly extend along the direction perpendicular to the applied field [shown by the dotted lines in Figs. 5(a) and 5(b)]. We also note that the bullet mode has a slightly smaller extent [a smaller "halo" is seen in Fig. 5(b)]. This is confirmed by our comparing the cross sections of the linearlike and bullet modes [Fig. 5(d)] extracted along the major axes of their profiles (as shown by the dotted lines in Figs. 5(a) and 5(b)]. The self-localization thus compresses the bullet mode's profile ever so slightly compared with the linearlike mode.

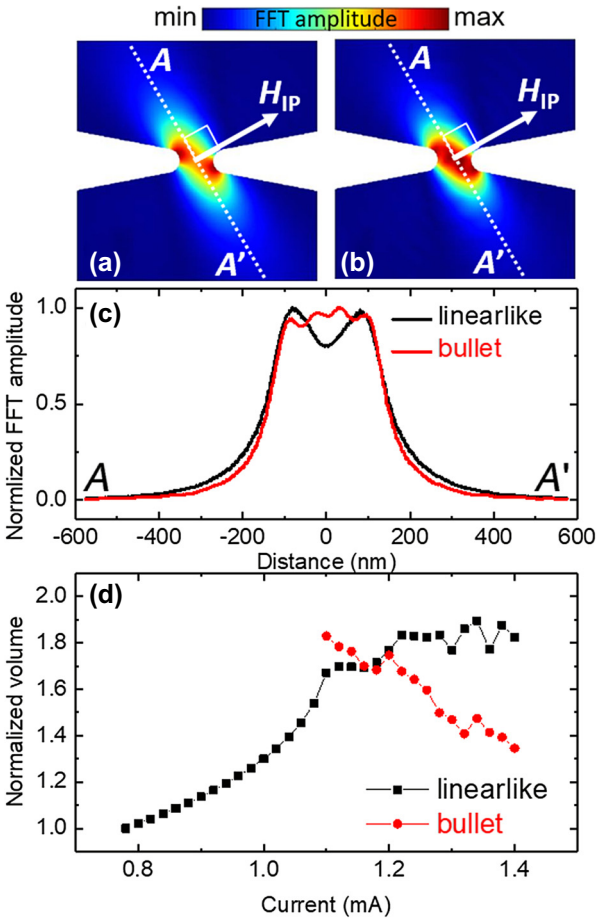

FIG. 5. (Simulation. The normalized mode profiles of the FFT peaks at $\mu_0 H_{IP} = 60$ mT, $\varphi = 30°$, and $I_{dc} = 1.26$ mA are shown in (a) for the linearlike mode confined to the edges of the nanoconstriction and in (b) for the bullet mode, which is more localized centrally in an area comparable to the constriction size. (c) FFT amplitude along the A-A' direction of the mode profiles perpendicular to the direction of the external field. (d) Normalized volumes of the linearlike mode (black rectangles) and the bullet mode (red circles) versus current.

To further highlight the different nature of the two modes, we estimate the spatial extent of the auto-oscillations versus applied current. For a given current value, we integrate the spatial profile of the auto-oscillation to extract the mode volume (as explained in Ref. [25]) and then normalize it by the value obtained at the onset

of the linearlike auto-oscillations. The results of our calculations are shown in Fig. 5(d). At first, while in the linearlike regime, the auto-oscillations undergo expansion and experience a slight, positive nonlinear frequency shift. This behavior is unique to the edge mode and is attributed to the recently predicted shallowing of the spin-wave wells with the precession amplitude [55]. At some current, the self-localization overcomes the delocalization and the linearlike auto-oscillations condense into the bullet, which then shrinks in monotonic fashion as its frequency redshifts with the applied current. It is worth mentioning that in extended films such nonmonotonic behavior of the auto-oscillations' volume and frequency can be observed only as a function of a strong oblique field [56].

We finally discuss how our results will have a direct impact on different applications of SHNOs. From a general perspective, our demonstration of operation at very low fields is important for most types of applications as the low field will allow operation in the static fields from thin-film permanent magnets. In addition, the very strong frequency tunability with field (Fig. 2) will make it possible to perform modulation not only via the drive current [57] but also independently via additional magnetic modulation fields [58], which can greatly increase the modulation rate. Similarly, only weak field changes will be required to switch from the first to the second harmonic (Fig. 3), which can allow ultrafast frequency-shift keying [50,59]. Although significant current tunability of spin-torque nano-oscillators and SHNOs is typically desirable for a number of applications, the somewhat-unexpected current-independent behavior of the linearlike mode in Fig. 2 could be useful in those cases where stability of the microwave generation with respect to drift or noise of the bias current is important. Detailed knowledge of the accessible spin-wave modes will also aid in the search for mutual synchronization in weak in-plane fields [27]. Being able to switch between different spin-wave modes with different extension and most likely very different synchronization properties, with use of either current or field, or a combination of both, will also provide a large degree of freedom when SHNOs are being explored for neuromorphic computing [23].

IV. CONCLUSION

We determine the dynamic magnetic properties of nanoconstriction-based SHNOs subject to weak in-plane magnetic fields by conducting microwave measurements and comparing the results obtain with the results of micromagnetic simulation of the same structure. We find that at high bias currents, the auto-oscillation spectra show two dominant modes: a linearlike mode that is confined to the edges of the constrictions, and a bullet mode that is confined to the center. While the former is a field-localized mode confined to the minima of the internal field, and therefore slightly depends on the strength of the current and its relative angle with regard to the external field, the frequency of the bullet mode rapidly decreases with its amplitude. Our simulations reveal that the two modes do not coexist at a given point in time, but instead mode hop, which also manifests itself in the experimentally observed linewidth broadening of the modes. Finally, our simulations show that the bullet nucleates from the linearlike mode and then experiences substantial auto-oscillation volume compression due to the nonlinear self-localization. Our findings provide a better understanding of the dynamics of nanoconstriction-based SHNOs necessary for subsequent studies of these systems, including their low-field operation and possible in-plane mutual synchronization.

ACKNOWLEDGMENTS

This work was supported by the Swedish Foundation for Strategic Research (SSF), the Swedish Research Council (VR), and the Knut and Alice Wallenberg foundation (KAW). This work was also supported by the European Research Council (ERC) under the European Union's Seventh Framework Programme (FP/2007-2013)/ERC Grant No. 307144 "MUSTANG."

[1] T. Chen, R. K. Dumas, A. Eklund, P. K. Muduli, A. Houshang, A. A. Awad, A. Dürrenfeld, B. G. Malm, A. Rusu, and J. Åkerman, Spin-torque and spin-Hall nano-oscillators, P. IEEE **104**, 1919 (2016).

[2] J. E. Hirsch, Spin Hall Effect, Phys. Rev. Lett. **83**, 1834 (1999).

[3] S. Zhang, Spin Hall Effect in the Presence of Spin Diffusion, Phys. Rev. Lett. **85**, 393 (2000).

[4] Y. K. Kato, R. C. Myers, A. C. Gossard, and D. D. Awschalom, Observation of the spin Hall effect in semiconductors, Science **306**, 1910 (2004).

[5] J. Wunderlich, B. Kaestner, J. Sinova, and T. Jungwirth, Experimental Observation of the Spin-Hall Effect in a Two-Dimensional Spin-Orbit Coupled Semiconductor System, Phys. Rev. Lett. **94**, 047204 (2005).

[6] E. Saitoh, M. Ueda, H. Miyajima, and G. Tatara, Conversion of spin current into charge current at room temperature: Inverse spin-Hall effect, Appl. Phys. Lett. **88**, 182509 (2006).

[7] S. O. Valenzuela and M. Tinkham, Direct electronic measurement of the spin Hall effect, Nature **442**, 176 (2006).

[8] V. E. Demidov, S. Urazhdin, H. Ulrichs, V. Tiberkevich, A. Slavin, D. Baither, G. Schmitz, and S. O. Demokritov, Magnetic nano-oscillator driven by pure spin current, Nat. Mater. **11**, 1028 (2012).

[9] R. H. Liu, W. L. Lim, and S. Urazhdin, Spectral Characteristics of the Microwave Emission by the Spin Hall Nano-oscillator, Phys. Rev. Lett. **110**, 147601 (2013).

[10] A. Zholud and S. Urazhdin, Microwave generation by spin Hall nanooscillators with nanopatterned spin injector, Appl. Phys. Lett. **105**, 2012 (2014).

[11] Z. Duan, A. Smith, L. Yang, B. Youngblood, J. Lindner, V. E. Demidov, S. O. Demokritov, and I. N. Krivorotov, Nanowire spin torque oscillator driven by spin orbit torques, Nat. Commun. **5**, 5616 (2014).

[12] M. Collet, X. de Milly, O. d'Allivy Kelly, V. V. Naletov, R. Bernard, P. Bortolotti, J. Ben Youssef, V. E. Demidov, S. O. Demokritov, J. L. Prieto, M. Muñoz, V. Cros, A. Anane, G. de Loubens, and O. Klein, Generation of coherent spin-wave modes in yttrium iron garnet microdiscs by spin-orbit torque, Nat. Commun. **7**, 10377 (2016).

[13] M. Ranjbar, P. Dürrenfeld, M. Haidar, E. Iacocca, M. Balinskiy, T. Q. Le, M. Fazlali, A. Houshang, A. A. Awad, R. K. Dumas, and J. Åkerman, CoFeB-based spin Hall nano-oscillators, IEEE Magn. Lett. **5**, 3000504 (2014).

[14] P. Dürrenfeld, A. A. Awad, A. Houshang, R. K. Dumas, and J. Åkerman, A 20 nm spin Hall nano-oscillator, Nanoscale **9**, 1285 (2017).

[15] C. f. Pai, L. Liu, Y. Li, H. W. Tseng, D. C. Ralph, and R. A. Buhrman, Spin transfer torque devices utilizing the giant spin Hall effect of tungsten, Appl. Phys. Lett. **101**, 122404 (2012).

[16] P. Dürrenfeld, F. Gerhard, M. Ranjbar, C. Gould, L. W. Molenkamp, and J. Åkerman, Spin Hall effect-controlled magnetization dynamics in NiMnSb, J. Appl. Phys. **117**, 17E103 (2015).

[17] H. Mazraati, S. Chung, A. Houshang, M. Dvornik, L. Piazza, F. Qejvanaj, S. Jiang, T. Q. Le, J. Weissenrieder, and J. Åkerman, Low operational current spin Hall nano-oscillators based on NiFe/Wbilayers, Appl. Phys. Lett. **109**, 242402 (2016).

[18] M. Zahedinejad, H. Mazraati, H. Fulara, J. Yue, S. Jiang, A. A. Awad, and J. Åkerman, CMOS compatible W/CoFeB/MgO spin Hall nano-oscillators with wide frequency tunability, Appl. Phys. Lett. **112**, 132404 (2018).

[19] T. M. Spicer, P. S. Keatley, T. H. J. Loughran, M. Dvornik, A. A. Awad, P. Dürrenfeld, A. Houshang, M. Ranjbar, J. Åkerman, V. V. Kruglyak, and R. J. Hicken, Spatial mapping of torques within a spin Hall nano-oscillator, arXiv:1805.00999v1 (2018).

[20] Y. Yin, P. Dürrenfeld, M. Dvornik, M. Ahlberg, A. Houshang, Y. Zhai, and J. Åkerman, Damping's effect on the magnetodynamics of spin Hall nano-oscillators, arXiv:1802.05548v1 (2018).

[21] V. E. Demidov, S. Urazhdin, A. Zholud, A. V. Sadovnikov, and S. O. Demokritov, Nanoconstriction-based spin-Hall nano-oscillator, Appl. Phys. Lett. **105**, 172410 (2014).

[22] A. A. Awad, P. Dürrenfeld, A. Houshang, M. Dvornik, E. Iacocca, R. K. Dumas, and J. Åkerman, Long-range mutual synchronization of spin Hall nano-oscillators, Nat. Phys. **13**, 292 (2017).

[23] J. Torrejon, M. Riou, F. A. Araujo, S. Tsunegi, G. Khalsa, D. Querlioz, P. Bortolotti, V. Cros, K. Yakushiji, A. Fukushima, H. Kubota, S. Yuasa, M. D. Stiles, and J. Grollier, Neuromorphic computing with nanoscale spintronic oscillators, Nature **547**, 428 (2017).

[24] M. Dvornik, A. A. Awad, P. Dürrenfeld, A. Houshang, E. Iacocca, R. K. Dumas, and J. Åkerman, Mutually synchronized spin Hall nano-oscillators for neuromorphic computing (Conference Presentation), Proc. SPIE **10357**, 1 (2017).

[25] M. Dvornik, A. A. Awad, and J. Åkerman, Origin of Magnetization Auto-oscillations in Constriction-based Spin Hall Nano-oscillators, Phys. Rev. Appl. **9**, 014017 (2018).

[26] A. Slavin and V. Tiberkevich, Nonlinear auto-oscillator theory of microwave generation by spin-polarized current, IEEE Trans. Magn. **45**, 1875 (2009).

[27] T. Kendziorczyk and T. Kuhn, Mutual synchronization of nanoconstriction-based spin Hall nano-oscillators through evanescent and propagating spin waves, Phys. Rev. B **93**, 134413 (2016).

[28] T. McGuire and R. Potter, Anisotropic magnetoresistance in ferromagnetic 3d alloys, IEEE Trans. Magn. **11**, 1018 (1975).

[29] J. C. Sankey, P. M. Braganca, A. G. F. Garcia, I. N. Krivorotov, R. A. Buhrman, and D. C. Ralph, Spin-Transfer-Driven Ferromagnetic Resonance of Individual Nanomagnets, Phys. Rev. Lett. **96**, 227601 (2006).

[30] J. C. Sankey, Y. T. Cui, J. Z. Sun, J. C. Slonczewski, R. A. Buhrman, and D. C. Ralph, Measurement of the spin-transfer-torque vector in magnetic tunnel junctions, Nat. Phys. **4**, 67 (2007).

[31] W. Chen, G. deLoubens, J.-M. L. Beaujour, J. Z. Sun, and A. D. Kent, Spin-torque driven ferromagnetic resonance in a nonlinear regime, Appl. Phys. Lett. **95**, 172513 (2009).

[32] X. Cheng, J. A. Katine, G. E. Rowlands, and I. N. Krivorotov, Nonlinear ferromagnetic resonance induced by spin torque in nanoscale magnetic tunnel junctions, Appl. Phys. Lett. **103**, 082402 (2013).

[33] M. Fazlali, M. Dvornik, E. Iacocca, P. Dürrenfeld, M. Haidar, J. Åkerman, and R. K. Dumas, Homodyne-detected ferromagnetic resonance of in-plane magnetized nanocontacts: Composite spin-wave resonances and their excitation mechanism, Phys. Rev. B **93**, 134427 (2016).

[34] L. Liu, T. Moriyama, D. C. Ralph, and R. A. Buhrman, Spin-Torque Ferromagnetic Resonance Induced by the Spin Hall Effect, Phys. Rev. Lett. **106**, 036601 (2011).

[35] C. Kittel, On the theory of ferromagnetic resonance absorption, Phys. Rev. **73**, 155 (1948).

[36] K. U. Demasius, T. Phung, W. Zhang, B. P. Hughes, S. H. Yang, A. Kellock, W. Han, A. Pushp, and S. S. P. Parkin, Enhanced spinorbit torques by oxygen incorporation in tungsten films, Nat. Commun. **7**, 10644 (2016).

[37] K. Ando, S. Takahashi, K. Harii, K. Sasage, J. Ieda, S. Maekawa, and E. Saitoh, Electric Manipulation of Spin Relaxation Using the Spin Hall Effect, Phys. Rev. Lett. **101**, 036601 (2008).

[38] H. Ulrichs, V. E. Demidov, S. O. Demokritov, W. L. Lim, J. Melander, N. Ebrahim-Zadeh, and S. Urazhdin, Optimization of Pt-based spin-Hall-effect spintronic devices, Appl. Phys. Lett. **102**, 132402 (2013).

[39] A. Slavin and V. Tiberkevich, Spin Wave Mode Excited by Spin-Polarized Current in a Magnetic Nanocontact is a Standing Self-Localized Wave Bullet, Phys. Rev. Lett. **95**, 237201 (2005).

[40] S. Bonetti, V. Tiberkevich, G. Consolo, G. Finocchio, P. Muduli, F. Mancoff, A. Slavin, and J. Åkerman, Experimental Evidence of Self-Localized and Propagating Spin Wave Modes in Obliquely Magnetized Current-Driven Nanocontacts, Phys. Rev. Lett. **105**, 217204 (2010).

[41] S. Bonetti, V. Puliafito, G. Consolo, V. S. Tiberkevich, A. N. Slavin, and J. Åkerman, Power and linewidth of propagating and localized modes in nanocontact spin-torque oscillators, Phys. Rev. B **85**, 174427 (2012).

[42] T. M. Spicer, P. S. Keatley, M. Dvornik, T. H. J. Loughran, A. A. Awad, P. Dürrenfeld, A. Houshang, M. Ranjbar, J. Åkerman, V. V. Kruglyak, and R. J. Hicken, Time resolved imaging of the non-linear bullet mode within an injection-locked spin Hall nano-oscillator, arXiv:1805.09212v1 (2018).

[43] M. B. Jungfleisch, W. Zhang, J. Sklenar, J. Ding, W. Jiang, H. Chang, F. Y. Fradin, J. E. Pearson, J. B. Ketterson, V. Novosad, M. Wu, and A. Hoffmann, Large Spin-Wave Bullet in a Ferrimagnetic Insulator Driven by the Spin Hall Effect, Phys. Rev. Lett. **116**, 057601 (2016).

[44] P. K. Muduli, O. G. Heinonen, and J. Åkerman, Decoherence and Mode Hopping in a Magnetic Tunnel Junction based Spin Torque Oscillator, Phys. Rev. Lett. **108**, 207203 (2012).

[45] P. K. Muduli, O. G. Heinonen, and J. Åkerman, Temperature dependence of linewidth in nanocontact based spin torque oscillators: Effect of multiple oscillatory modes, Phys. Rev. B **86**, 174408 (2012).

[46] E. Iacocca, O. Heinonen, P. K. Muduli, and J. Åkerman, Generation linewidth of mode-hopping spin torque oscillators, Phys. Rev. B **89**, 054402 (2014).

[47] O. G. Heinonen, P. K. Muduli, E. Iacocca, and J. Åkerman, Decoherence, mode hopping, and mode coupling in spin torque oscillators, IEEE Trans. Magn. **49**, 4398 (2013).

[48] R. Sharma, P. Dürrenfeld, E. Iacocca, O. G. Heinonen, J. Åkerman, and P. K. Muduli, Mode-hopping mechanism generating colored noise in a magnetic tunnel junction based spin torque oscillator, Appl. Phys. Lett. **105**, 132404 (2014).

[49] V. Tiberkevich and A. Slavin, Nonlinear phenomenological model of magnetic dissipation for large precession angles: Generalization of the Gilbert model, Phys. Rev. B **75**, 014440 (2007).

[50] P. K. Muduli, O. G. Heinonen, and J. Åkerman, Intrinsic frequency doubling in a magnetic tunnel junction based spin torque oscillator, J. Appl. Phys. **110**, 076102 (2011).

[51] A. Vansteenkiste, J. Leliaert, M. Dvornik, M. Helsen, F. Garcia-Sanchez, and B. Van Waeyenberge, The design and verification of MuMax3, AIP Adv. **4**, 107133 (2014).

[52] J. M. D. Coey, *Magnetism and Magnetic Materials* (Cambridge University Press, Cambridge, England, 2010).

[53] M. Dvornik, Ph.D. thesis, University of Exeter, 2011, https://ore.exeter.ac.uk/repository/handle/10036/3304.

[54] M. Dvornik, Y. Au, and V. V. Kruglyak, *Micromagnetic Simulations Inmagnonics*, edited by Sergej O. Demokritov and Andrei N. Slavin, Topics in Applied Physics, Vol. 125 (Springer Nature, Exeter, United Kingdom, 2013), p. 101.

[55] M. Dvornik and J. Åkerman, Anomalous nonlinearity of the magnonic edge mode, arXiv:1804.01585 (2018).

[56] A. N. Slavin and P. Kabos, Approximate theory of microwave generation in a current-driven magnetic nanocontact magnetized in an arbitrary direction, IEEE Trans. Magn. **41**, 1264 (2005).

[57] M. Zahedinejad, A. A. Awad, P. Dürrenfeld, A. Houshang, Y. Yin, P. K. Muduli, and J. Åkerman, Current modulation of nanoconstriction spin-Hall nano-oscillators, IEEE Magn. Lett. **8**, 3704804 (2017).

[58] A. Purbawati, F. Garcia-Sanchez, L. D. Buda-Prejbeanu, and U. Ebels, Enhanced modulation rates via field modulation in spin torque nano-oscillators, Appl. Phys. Lett. **108**, 122402 (2016).

[59] H. S. Choi, S. Y. Kang, S. J. Cho, I. Y. Oh, M. Shin, H. Park, C. Jang, B. C. Min, S. I. Kim, S. Y. Park, and C. S. Park, Spin nano-oscillator-based wireless communication, Sci. Rep. **4**, 1 (2014).